Environmental Science Advances

ROYAL SOCIETY OF CHEMISTRY

PAPER

View Article Online
View Journal | View Issue

Cite this: *Environ. Sci.: Adv.*, 2025, **4**, 1514

Pore-water electrical conductivity assessment: an integrated ground-penetrating radar–electromagnetic induction approach

Sashini Pathirana, *[a] Sébastien Lambot,[b] Manokararajah Krishnapillai,[a] Mumtaz Cheema,[a] Christina Smeaton[a] and Lakshman Galagedara *[a]

Pore-water electrical conductivity (ECw) is the ideal indicator of soil salinity in agriculture, as it directly represents the salinity experienced by plant roots. However, its practical application is limited by its dependence on soil water content and the labour-intensive, destructive, costly, and time-consuming process of pore-water extraction and analysis, especially for large-scale field applications. Ground-penetrating radar (GPR) and electromagnetic induction (EMI) provide non-destructive, time-efficient, and cost-effective alternatives for estimating soil properties and state variables. This study aimed to develop a method for estimating ECw by integrating GPR and EMI techniques using both stochastic and deterministic approaches at the field scale. EMI and GPR surveys were conducted before and after controlled irrigations, and soil samples were collected for laboratory analysis as ground truthing. The stochastic approach involved developing multiple linear regression (MLR) models, whereas the deterministic approach involved modifying and evaluating Archie's equation. The MLR models demonstrated high predictive accuracy, with an R^2 of 0.75 between measured and predicted ECw values. Both approaches provided reliable ECw predictions, with low root mean square error (RMSE) during evaluation (<1.67 mS m^{-1} for MLR and <2.65 mS m^{-1} for Archie's equation). However, the parameters in Archie's equation deviated from laboratory-estimated values and required modifications. At the study site, the stochastic approach outperformed the deterministic approach. Future research should focus on refining these models to improve their applicability across different soil types and conditions, aiming to improve the accuracy and reliability of soil salinity assessments in various agricultural landscapes.

Received 4th May 2025
Accepted 28th July 2025

DOI: 10.1039/d5va00121h

rsc.li/esadvances

Environmental significance

Soil salinity has become a major issue in agriculture globally, impacting crop productivity and sustainability. Assessment of pore-water electrical conductivity (ECw)—a direct indicator of root-zone salinity—is crucial in precision agriculture and challenging to estimate in the agricultural landscape with traditional methods. Efficient, non-invasive salinity monitoring is key for managing soil health, optimizing irrigation, crop productivity, and ensuring long-term agricultural sustainability. This study demonstrates the potential and challenges of a novel, non-invasive approach for estimating ECw at the field-scale by integrating ground-penetrating radar (GPR) and electromagnetic induction (EMI) techniques with both stochastic and deterministic methods. These findings support the development of field-scale tools for salinity monitoring, offering a pathway toward improved soil and water management in precision agriculture.

1 Introduction

Soil salinity, the concentration of soluble salts in the soil, plays a critical role in seed germination, plant growth and overall agricultural productivity.[1] Excessive salinity disrupts plant development by damaging roots, reducing yields, and, in severe cases, causing plant mortality, posing a significant threat to global food security. The excessive salt concentrations lower the osmotic soil potential, making water uptake difficult for plants, even in well-irrigated conditions. This results in physiological drought, ion toxicity, altered soil permeability, and nutrient imbalances.[1,2] Salinity build-up in agricultural soils is primarily driven by the combined effect of insufficient drainage due to limited precipitation or irrigation, as well as evapotranspiration, which removes water while leaving salts behind, thereby increasing ion concentrations. Furthermore, fertilizers, soil amendments, and irrigation (saline water) introduce extra ions into the soil.[1–3]

[a]*School of Science and the Environment, Memorial University of Newfoundland, Corner Brook, Newfoundland and Labrador, Canada. E-mail: epspathirana@mun.ca; lgalagedara@mun.ca*

[b]*Earth and Life Institute, Université catholique de Louvain, 1348 Louvain-la-Neuve, Belgium*

Soil salinity results from the presence of inorganic dissolved substances in the soil's aqueous phase, including various dissolved and readily dissolvable ions (such as Na^+, K^+, Mg^{2+}, Ca^{2+}, Cl^-, HCO_3^-, NO_3^-, SO_4^{2-}), as well as ion complexes. Since these substances conduct electricity, salinity is often expressed in terms of electrical conductivity (EC), which measures the ability of soil to conduct an electrical current.[4–10] The more ions are present in the pore water, the higher its EC; consequently, the higher the bulk electrical conductivity of the soil.

Several methods have been developed and tested for determining soil salinity at field scales, including visual crop observation, soil solution EC (pore-water electrical conductivity – ECw), time domain reflectometry (TDR), electrical resistivity, and electromagnetic induction (EMI).[1,10] Visual crop observations, though quick and cost-effective, are subjective and only detect salinity after visible crop damage. Advances in remote sensing offer the potential for early detection of plant stress before it becomes evident. Soil salinity estimation traditionally involves soil sampling followed by laboratory analysis, such as extracting soil water/solution and measuring its EC. While accurate, these methods are labour-intensive, time-consuming, destructive, and provide limited spatial coverage for large-scale field applications.[1,8]

TDR measures EC at a point scale but has limited field-scale applicability. However, its ability to simultaneously measure soil moisture through dielectric permittivity makes it vulnerable to integrated salinity assessments.[1] Electrical resistivity and EMI provide *in situ* alternatives for salinity measurement. Electrical resistivity allows for flexible depth adjustments depending on electrode spacing, but it is destructive, time-consuming, and less effective in dry or rocky soils. Off-ground EMI offers rapid, non-invasive assessments over large areas and allows flexible depth adjustments depending on coil orientation and spacing. For both electrical resistivity and EMI, the measured values correspond to depth-weighted apparent electrical conductivity (ECa). However, depth-dependent conductivity profiles can be reconstructed using tomographic inversion. In all cases, these methods need calibration for accurate salinity estimation, as ECa is influenced by multiple factors, including soil texture (*e.g.*, clay content), mineralogy, soil water content (SWC), porosity or bulk density, soil structure, and temperature.[1,4,5,7,10]

Theoretically, ECw is the most accurate measure of soil salinity for agriculture, as it directly represents the salinity experienced by plant roots, which is crucial for understanding the impact on crop health and productivity.[1] Despite its importance and direct salinity measurement, ECw is not widely used in practice due to several challenges, such as fluctuations during irrigation with SWC changes, making it difficult to obtain consistent measurements.[1] Additionally, traditional methods for collecting soil solution/pore-water are labour-intensive, costly and destructive, especially at typical field water contents, which makes large-scale field applications impractical.[9,11]

Near-surface geophysical techniques such as EMI and ground-penetrating radar (GPR) have emerged as promising techniques to estimate soil properties and state variables such as SWC,[12–23] soil salinity,[24–26] organic matter/carbon,[26–29] and compaction/bulk density.[30–34] These techniques offer non-destructive, efficient, and cost-effective estimations of soil properties and state variables in agricultural landscapes compared to the traditional methods.[35]

Several studies have demonstrated the potential of GPR and EMI methods for estimating soil salinity and related parameters using both empirical and modeling approaches. In GPR, early-time amplitude analysis under uniform hydraulic conductivity and saltwater conditions revealed a strong correlation between GPR reflected wave amplitude and salinity levels.[36] Another study employed reflection coefficient methods and waveform comparison under varying conductivity conditions to detect salinity variations.[37] In the case of EMI, several investigations have successfully developed simple linear and multiple regression models linking EMI-measured ECa to measured ECe. For example, high correlations ($R^2 > 0.90$) were reported using EM38 and GEM300 instruments.[38] Similarly, models estimating soil salinity and sodium adsorption ratio (SAR) achieved strong correlations ($R^2 = 0.89$–0.93) at different field sites.[39] Recent advances have further highlighted EMI's value for salinity monitoring by applying time-lapse inversion of EMI data integrated with HYDRUS-2D modeling to assess temporal salinity dynamics under saltwater irrigation. The study reported a strong correlation (correlation coefficient (r) = 0.88) between ECa and ECe.[40] Another study utilized HYDRUS-2D simulations to optimize EMI sensor placement in drip-irrigated soils, identifying irrigation water salinity as the primary factor influencing ECa and ECe distributions.[41] Time-lapse EMI inversion was employed with site-specific calibration to map salinity changes over time, achieving high mapping accuracy (coefficient of determination (R^2) = 0.81).[42] A recent study developed a deep learning-based model to invert EMI data and integrate it with HYDRUS-1D simulations, efficiently modeling water-salt transport dynamics in arid zones.[43] However, to the best of our knowledge, there remains a gap in research that integrates GPR and EMI methods for soil salinity assessment. Specifically, no existing studies have focused on the field-scale estimation of ECw using GPR, EMI or an integrated GPR–EMI approach.

EMI is particularly effective in estimating ECa, although its accuracy in predicting ECw is limited due to the strong influence of SWC, clay content, and soil structure.[1] Conversely, GPR has been well-established for estimating SWC over the past three decades.[15,16,35] By integrating GPR and EMI, it is promising to improve field-scale salinity estimation, as GPR detects SWC variations while EMI captures ECa fluctuations related to salinity.[44]

Various approaches, including stochastic and deterministic methods, have been applied in the literature to estimate soil salinity (as EC of the saturated paste extract – ECe) from ECa. The stochastic approach involves statistical modeling, while the deterministic approach relies on theoretical or empirical models. While relationships between ECa and ECw are well established in Archie's equation and Rhoade's equation, this study presents a novel integration of GPR and EMI for estimating ECw at the field scale. Possible deterministic

approaches for estimating ECw using integrated EMI-GPR data include Archie's equation,[45] which relates ECa to porosity, soil water saturation (Sw) and ECw, and Rhoades's model,[9,46,47] which incorporates SWC, ECw and solid phase conductivity (ECs).

This study aims to develop and evaluate methods for non-destructive ECw estimation at the field scale using integrated GPR and EMI. The research intends to support precision agriculture by providing accurate and spatially detailed soil salinity assessments for optimizing irrigation and soil management practices (water and solute transport). The study hypothesizes that integrating GPR and EMI with deterministic or stochastic approaches will provide a reliable method for non-destructive ECw estimation at the field scale. This hypothesis was tested through a field experiment, which adapted theoretical approaches previously validated in laboratory settings and developed multiple linear regression (MLR) models.

The specific objectives of this study were: (1) to develop and evaluate MLR models for estimating ECw using integrated GPR–EMI data (stochastic approach); (2) to apply and assess petrophysical models, specifically Archie's and Rhoades' equations, for ECw estimation based on GPR–EMI data (deterministic approach); and (3) to compare the effectiveness of the stochastic and deterministic approaches for ECw estimation at the study site.

2 Theoretical background

2.1. Rhoades's equation

Rhoades's equation assessed the soil bulk ECa, considering two parallel pathways for current flow: one through the soil solution and the other through the electrical double layer.[47] The soil water EC and the bulk surface electrical conductivity, which are primarily affected by exchangeable cations adsorbed onto clay minerals, are key components in this model. Rhoades's equation incorporates the influence of the soil matrix, making it particularly useful in heterogeneous soils where the matrix has a significant impact on overall conductivity,[9,46,47] shown in eqn (1).

$$\mathrm{ECa} = \mathrm{ECw} \times \theta \times T + \mathrm{ECs} \quad (1)$$

Where ECa is the apparent electrical conductivity, ECw is the pore-water electrical conductivity, θ is the volumetric soil water content, T is the transmission coefficient, and ECs is the solid phase electrical conductivity.

T accounts for the impedance of current flow through soil water in void spaces and the reduced mobility of ions near the solid–liquid interface. T, which is always less than or equal to 1, corresponds to the ratio of the straight-line length (l) to the path length of the electrical current (l_e), effectively the reciprocal of the electrical conductivity tortuosity factor (l_e/l).[9,46,47] The model can also be expressed through parameters a and b, which vary between soils and are determined by fitting the model to observed data as shown in eqn (2). Other researchers also have documented linear relationships between T and θ.[48,49]

$$T = a \times \theta + b \quad (2)$$

2.2. Archie's equation

Two empirical relationships through laboratory experiments were developed to relate apparent electrical conductivity (ECa), soil water saturation (Sw), pore water electrical conductivity (ECw), and porosity (φ) in porous rocks, particularly in petroleum engineering.[45] The first equation was designed for fully saturated porous rocks, while the second was intended for partly saturated conditions. These relationships introduce the saturation exponent (n) and the cementation exponent (m) as key parameters. Over time, Archie's equation has been adapted for use in soils.[50–53] The general form of Archie's equation for soils is shown in eqn (3).

$$\mathrm{ECa} = \phi^m \mathrm{Sw}^n \mathrm{ECw} \quad (3)$$

In soil science, Archie's equation is valuable for modeling the relationship between the soil's electrical properties, SWC, and salinity. However, the equation's parameters must be calibrated for different soil types, as factors like soil texture and compaction, porosity and Sw can significantly influence the conductivity. In this study, we intentionally chose to use the original Rhoades and Archie equations to maintain consistency with foundational approaches and to evaluate their applicability under the specific field conditions.

3 Methodology

3.1. Study area

The field experiment was conducted at the Western Agriculture Center and Research Station in Pynn's Brook (49° 04′20″N, 57° 33′35″W), Pasadena, Newfoundland and Labrador, Canada. The site is managed by the Department of Fisheries, Forestry, and Agriculture of the Government of Newfoundland and Labrador. The average composition (number of samples = 30) of key soil properties at a depth of 0–60 cm in the study site included gravel at 30.5% (±4.97%), sand at 86.8% (±4.98%), silt at 10.7% (±4.24%), clay at 2.5% (±0.91%), and soil organic matter at 3.8% (±2.05%).[54]

3.2. Field data collection

A 12 m × 9 m area was selected, comprising two experimental blocks (Fig. 1a). Each block contained three 2 m × 3 m sub-plots designated for saltwater (SW) irrigation. Within each sub-plot, three soil sampling locations were identified as replicates, totalling 18 sampling locations across blocks 1 and 2 (Fig. 1a). A total of 60 L of SW was prepared by dissolving 240 g of table salt (NaCl) in freshwater (EC = 1 mS m^{-1}). SW irrigation was applied to increase the EC in the soil solution, and table salt was selected since it is a commonly available salt (Na^+ and Cl^-) in the soil and agricultural inputs. The SW was manually applied, as uniformly as possible, using a watering can to each sub-plot during two irrigation events (irrigation 1 and 2), with the second irrigation applied three hours after the first. EMI and GPR

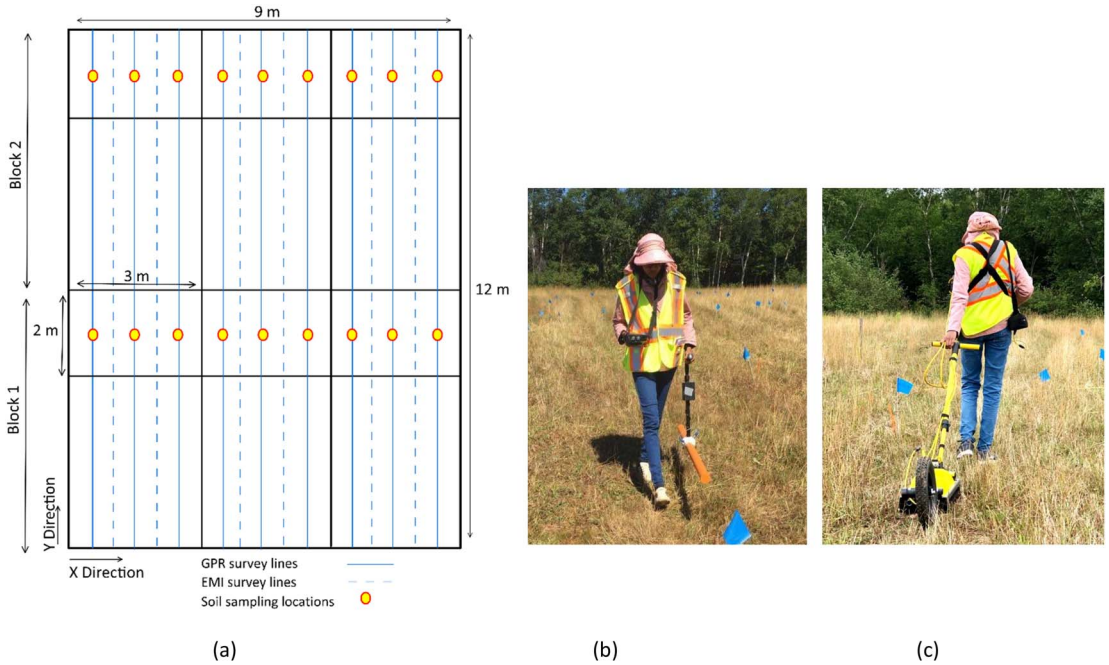

Fig. 1 (a) Field diagram showing the data collection system and plots, and geophysical surveys (b) electromagnetic induction (EMI), and (c) ground-penetrating radar (GPR).

surveys, along with soil sampling, were conducted in three stages: (1) before irrigation as background (BKG), (2) after the end of irrigation 1 (EOI-1), and (3) after the end of irrigation 2 (EOI-2).

EMI surveys were conducted in the continuous mode using a multi-coil EMI sensor (CMD-MINIEXPLORER, GF instruments, Czech Republic) with an operating frequency of 30 kHz (Fig. 1b). Prior to each survey, the instrument was warmed up for a minimum of 30 min. Surveys were carried out separately for vertical coplanar (VCP) and horizontal coplanar (HCP) coil orientations. Instrumental drift in ECa measurements was not anticipated due to the high stability of the instrument concerning temperature variations (Guide for Electromagnetic Conductivity Mapping and Tomography – GF instruments). To maintain consistency, the instrument was operated using a handle at an average height of 0.20 m above the ground by the same person throughout the experiment to maintain a relatively constant height and speed. Coils 2 and 3, which measure depths beyond the study's sampling range of ~0–0.30 m, were excluded from further analysis. VCP and HCP are hereafter used to refer to ECa measurements from vertical coplanar coil one, respectively.

GPR data were acquired using a 500 MHz center-frequency transducer (PulseEKKOPro, Sensors and Software, Canada) (Fig. 1c). A fixed-offset survey method was employed, with an antenna separation of 0.23 m, a step size of 0.05 m, a time window of 50 ns, and 32 stacks. EMI surveys were conducted at 0.5 m intervals along the *X* direction, resulting in 19 survey lines per data collection stage (Fig. 1a). GPR survey lines were spaced at 1 m intervals, offset by 0.5 m along the *X* direction, totalling nine survey lines (Fig. 1a).

Both undisturbed and disturbed soil samples were collected to facilitate various laboratory analyses. Undisturbed samples were collected down to a depth of 0.30 m at the BKG to estimate bulk density, which was subsequently used to calculate soil porosity. This measurement (BKG) was assumed to remain stable throughout the experiment. Disturbed soil samples were also collected down to a depth of 0.30 m to determine ECw in the laboratory at BKG, EOI-1 and EOI-2 stages from sampling locations shown in Fig. 1a. This approach allowed for the assessment of temporal changes in ECw corresponding to SW irrigation.

3.3. Data processing

Since soil temperature influences subsurface electrical properties, including ECa measured *via* EMI, data were corrected to a reference temperature of 25 °C to eliminate temperature-induced variability across different stages (measured soil temperature: BKG −19.03 °C, EOI-1 −26.47 °C, and EOI-2 −30.27 °C) using eqn (4) and (5).[55]

$$EC_{25} = f_t \times EC_t \quad (4)$$

$$f_t = 0.4470 + 1.4034e^{\frac{-t}{26.815}} \quad (5)$$

where EC_{25} is the EC at 25 °C; f_t is the temperature conversion factor; t is the measured temperature in Celsius; EC_t is the EC measured at the temperature t.

The GPR data were time-zero corrected and processed by applying filters. Direct ground wave travel times were picked using the assisted pick processing tool in PulseEKKO Project V5R3 software and converted to direct ground wave velocities. Then, volumetric SWCs were calculated by using eqn (6) and (7).[56]

$$K_r = \left(\frac{c}{V_{DGW}}\right)^2 \quad (6)$$

$$SWC = -5.3 \times 10^{-2} + 2.92 \times 10^{-2}\,Kr - 5.5 \times 10^{-4}\,Kr^2 + 4.3 \times 10^{-6}\,Kr^3 \quad (7)$$

Ordinary (point) kriging was used to create interpolated maps from temperature-corrected ECa and GPR-estimated SWCs. Data points were digitized to match the soil sampling shown in Fig. 1a to obtain ECa and SWC data for analysis. Soil porosity was calculated using measured bulk density values, and Sw at each location and stage was determined by using the GPR-estimated SWCs and calculated porosity.

3.4. Data analysis

Descriptive statistics were used to evaluate data distribution and variability. A one-way analysis of variance (one-way ANOVA) was performed to assess the effect of irrigation on EMI measurements (VCP and HCP), GPR-estimated SWC and calculated Sw. The null hypothesis assumed that the group means of BKG, EOI-1, and EOI-2 were equal at a 0.05 significance level.

Field data analysis was structured around two approaches: stochastic and deterministic. For objective 1, the stochastic approach involved developing MLR models to predict ECw using data from Block 1 (Fig. 2). Separate MLR models were developed for VCP and HCP data. Model evaluation was performed using data from Block 2 by comparing the predicted and measured ECw values through a 1 : 1 line analysis and calculating the root mean square error (RMSE) (Fig. 2).

For objective 2, the deterministic approach involved visualizing the field data and applying Rhoades's and Archie's equations to data from both Block 1 and Block 2 (Fig. 2). Two models were considered for each petrophysical relationship using VCP and HCP data. Further analysis was conducted under the deterministic approach based on graphical trends. Archie's equation was specifically applied to data from Block 1 using calculated porosity, Sw, and measured ECw to estimate ECa. Initially, literature-based exponent values (m and n) were used, but these parameters were later optimized using the solver function in Microsoft Excel to minimize the error between the ECa measured by EMI and the ECa calculated using Archie's equation. The optimized parameters were then applied to predict ECw using the data from Block 2 (Fig. 2). The accuracy was evaluated using a 1 : 1 line comparison and RMSE.

To compare the stochastic (MLR) and deterministic (Archie's equation) approaches for estimating ECw in field applications, F-statistics were calculated, and Bland–Altman plots were generated between measured and predicted values (from both MLR and Archie's equation) (Fig. 2).

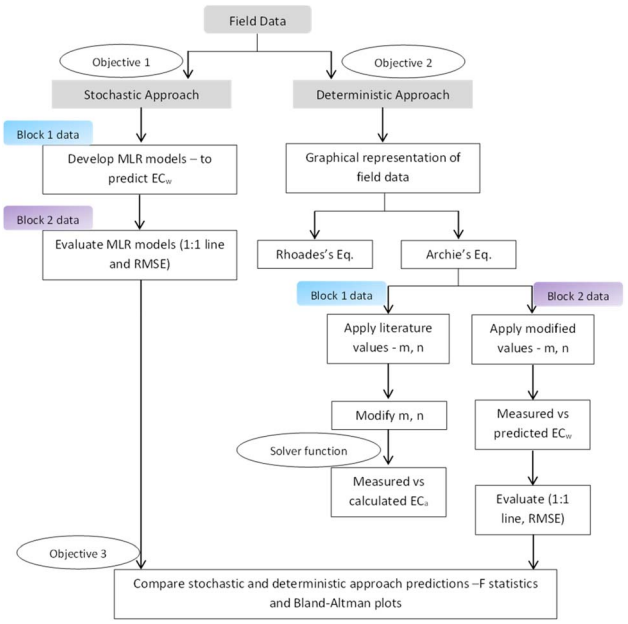

Fig. 2 Flow chart of the field data analysis using stochastic approach and deterministic approach.

4 Results and discussion

4.1. Descriptive statistics

The descriptive statistics for data from Blocks 1 and 2 indicate that the mean values, standard deviations, and ranges are relatively similar across both blocks (Table 1). Furthermore, the datasets follow a normal distribution, as evidenced by the skewness and kurtosis values being close to zero (Table 1).

The ANOVA results (Table 2) revealed significant differences ($p < 0.001$, $\alpha = 0.05$) among the BKG and the two irrigation events (EOI-1 and EOI-2) across all measured variables in Blocks 1 and 2. The mean SWC was significantly different between BKG

Table 1 Descriptive statistics of studied variables in Block 1 and Block 2

		Block 1						Block 2					
Variables	n	Mean	St. Dev	Min	Max	Kurtosis	Skewness	Mean	St. Dev	Min	Max	Kurtosis	Skewness
SWC (cm m^{-1})	27	22.1	8.4	9.4	34.6	−1.4	−0.5	23.22	7.33	8.30	30.63	−1.2	−0.6
VCP (mS m^{-1})	27	3.52	1.91	0.99	7.10	−1.1	0.0	2.06	1.03	0.51	4.12	−1.1	0.3
HCP (mS m^{-1})	27	4.11	1.55	2.35	6.41	−1.5	0.2	2.94	1.26	1.48	5.18	−1.3	0.5
ECw (mS m^{-1})	27	5.13	3.44	0.67	10.75	−1.3	0.0	4.14	2.66	0.55	10.08	−0.9	0.3
Sw (%)	27	45.4	16.8	20.0	66.6	−1.5	−0.6	42.18	13.57	17.05	64.02	−1.2	0.1
Porosity (%)	9	47.9	0.94	44.0	53.5	0.7	0.7	49.0	0.81	46.3	54.3	0.5	0.8

Table 2 Results of one-way analysis of variance (ANOVA) and Tukey tests for background (BKG) after first irrigation (EOI-1) and after second irrigation (EOI-2)[a]

Variables	BKG	EOI-1	EOI-2	*F*-value	*p*-value
SWC_{GPR} (cm m^{-1})	12.29[b]	26.84[a]	28.81[a]	240.34	0.000
VCP (mS m^{-1})	1.042[c]	3.08[b]	4.19[a]	34.66	0.000
HCP (mS m^{-1})	2.06[c]	3.25[b]	5.24[a]	82	0.000
ECw (mS m^{-1})	1. 05[c]	5.07[b]	7.77[a]	113.81	0.000
Sw (%)	25.14[c]	48.09[b]	58.12[a]	131.93	0.000

[a] Null hypothesis: all means are equal; $\alpha = 0.05$; DF = 53; letters a, b, and c indicate significant differences within each stage of BKG, EOI-1 and EOI-2 based on Tukey's tests.

and the post-irrigation stages (EOI-1 and EOI-2), although no significant difference was observed between EOI-1 and EOI-2. For the other variables (VCP, HCP, ECw, and Sw), the lowest mean values were found at BKG, with progressive increases in EOI-1 and EOI-2, showing significant differences across all three stages. Overall, these ANOVA results confirm that all variables responded to the applied irrigation. Spatial variability of GPR estimated Kr and EMI measured ECa shown in the Appendix (Fig. 9 and 10).

4.2. Stochastic approach

The MLR models for predicting ECw identified ECa and Sw as the most significant predictors. Although porosity was initially considered a potential predictor during model development, it was eventually excluded from the final models due to its limited contribution to prediction accuracy. Instead, the final models incorporated both VCP and HCP, which were found to be more relevant for accurate predictions. The variance inflation factor (VIF) for the VCP-based MLR model was less than 5 for both VCP and Sw, indicating no multicollinearity among the dependent variables (Table 3). However, the HCP-based MLR model exhibited moderate multicollinearity, with VIF values under 10 for HCP and Sw (Table 3). While this level of multicollinearity does not compromise the validity of the model, it may reduce the stability and interpretability of the individual regression coefficients, making it challenging to isolate the effect of each predictor on ECw. We acknowledge this limitation when interpreting the role of closely correlated predictors. Future research may benefit from applying multicollinearity-mitigating techniques, such as ridge regression, to improve model robustness and enhance interpretability. The developed MLR models

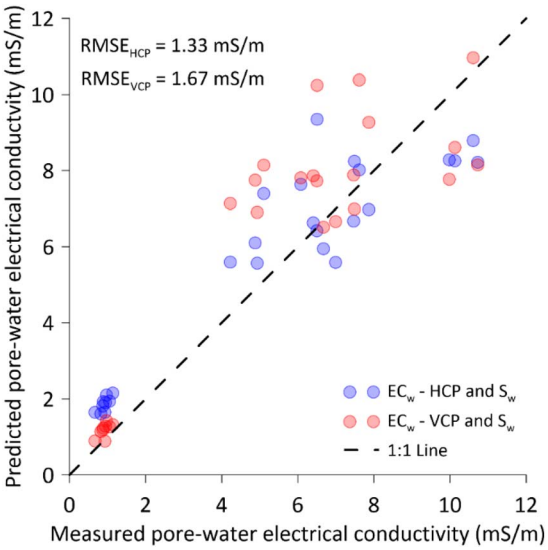

Fig. 3 Scatter plots of measured *versus* regression models (MLR) predicted pore-water electrical conductivity (ECw). The dash line corresponds to the 1 : 1 line.

demonstrate high R^2 values and low RMSE, as detailed in Table 3. The inclusion of both ECa and Sw in the MLR models highlights their importance in predicting the ECw.

Evaluation of the developed MRL models revealed acceptable prediction accuracy, with most data points aligning closely or scattering around the 1 : 1 line (Fig. 3). Under the BKG conditions, the predicted ECw values closely matched the observed values, indicating strong agreement. However, following irrigation, predictions become more dispersed, exhibiting increased variability and reduced consistency in matching observed ECw values. This suggests that irrigation introduces variability likely due to the sudden influx of ions from SW and non-uniform wetting patterns, impacting model performance compared to the stable baseline conditions (Fig. 3). Despite this, the VCP and HCP-based MLR models effectively predicted ECw. The HCP-based MLR model achieved a lower RMSE value of 1.33 mS m^{-1} compared to 1.67 mS m^{-1} for the VCP-based model (Fig. 3).

4.3. Deterministic approach

Three-dimensional surface plots illustrate ECw (*X*-axis) and SWC (*Y*-axis), with ECa values measured by EMI shown on the *Z*-axis (Fig. 4). Subplots are provided for both coil orientations: (a)

Table 3 Summary of the developed multiple linear regression models, including their predictive capabilities

Regression equation	R^2	RMSE (mS m^{-1})	*p*-value	VIF
ECw = −2.06 + 1.02 VCP + 9.52 Sw	0.75	1.35	0.000	VCP −4.35 Sw −4.28
ECw = −2.28 + 0.84 HCP + 9.34 Sw	0.74	1.41	0.000	HCP −7.06 Sw −6.98

VCP and (b) HCP. The ECa values exhibit a clear dependence on both ECw and SWC (Fig. 4). At low SWC, ECa increases more linearly with ECw, whereas at high ECw, ECa shows a more linear increase with SWC. This behaviour reflects the combined influence of ionic concentration and SWC on the soil's bulk EC, as both factors enhance the continuity and conductivity of the pore water phase. Interestingly, the HCP configuration yields higher ECa values than the VCP configuration. Overall, the shape of the measured surface closely aligns with the trends predicted by Rhoades's petrophysical model, supporting its physical relevance under field conditions.

A previous laboratory experiment by Rhoades *et al.*[46] found that in loam soils, ECa–ECw curves diverged with increasing SWC once ECw exceeded ~50 mS m^{-1}, with the curve slope increasing at higher SWCs. However, in this study, no such divergence was observed across different irrigation stages, likely because field-measured ECa and ECw remained below 50 mS m^{-1} throughout the study (Appendix (Fig. 11)). This limited data range constrains a more detailed exploration of these relationships and is removed from further analysis in this paper.

The relationship between field-measured ECa from EMI and Sw is illustrated in Fig. 5. Both measured and calculated ECa data follow a distinct power-law relationship, consistent with Archie's model (eqn (3)). EMI-measured ECa values (represented by dots for VCP and HCP) and those calculated using Archie's model exhibit a non-linear positive response to increasing Sw levels. This trend highlights the sensitivity of ECa to variations in Sw and ECw, as higher water saturation and the introduction of salts lead to elevated ECa values. The strong agreement between the measured and calculated ECa further validates Archie's model in describing the field-measured ECa values.

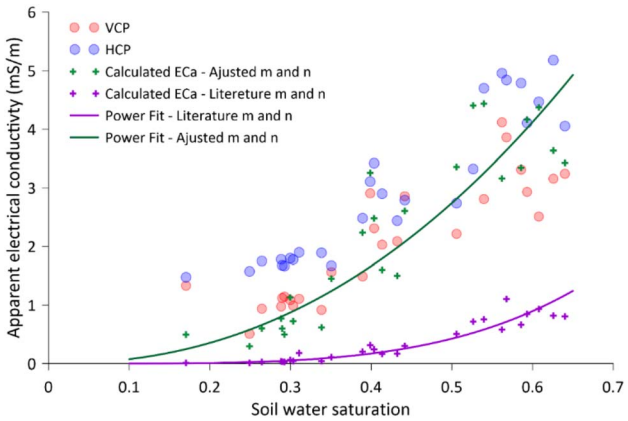

Fig. 5 Apparent electrical conductivity (ECa) as a function of soil water saturation (Sw), based on Archie's petrophysical model. The circle symbol shows the electromagnetic induction (EMI) measured ECa (VCP, HCP), and the cross symbol shows the calculated ECa using Archie's model (model parameters from literature and adjusted based on measured field data).

Using the literature-suggested exponents ($m = 1.5$, $n = 2$) for sandy soils in Archie's equation resulted in a noticeable underestimation of ECa compared to the EMI-measured ECa from both VCP and HCP modes. To improve the accuracy, a solver function minimized the RMSE between measured ECa and Archie's model predictions, yielding optimized exponents of $m = 0.67$ and $n = 0.11$. These adjustments reduced RMSE to 0.99 mS m^{-1} for VCP and 0.98 mS m^{-1} for HCP mode, as shown in Fig. 6. Although these optimized exponents deviate significantly from typical values for sandy soils in laboratory settings, they improved the model's predictive accuracy. The optimized

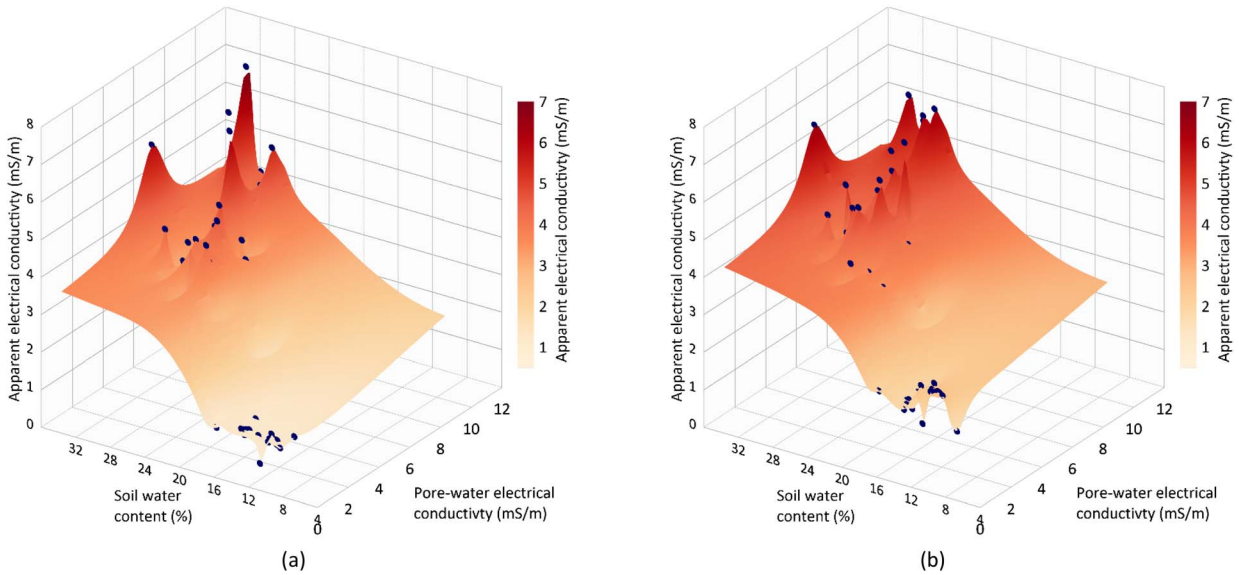

Fig. 4 3D surface plot for measured pore-water electrical conductivity (ECw) and soil water content (SWC), apparent electrical conductivity (ECa) measured from electromagnetic induction (EMI); (a) VCP and (b) HCP.

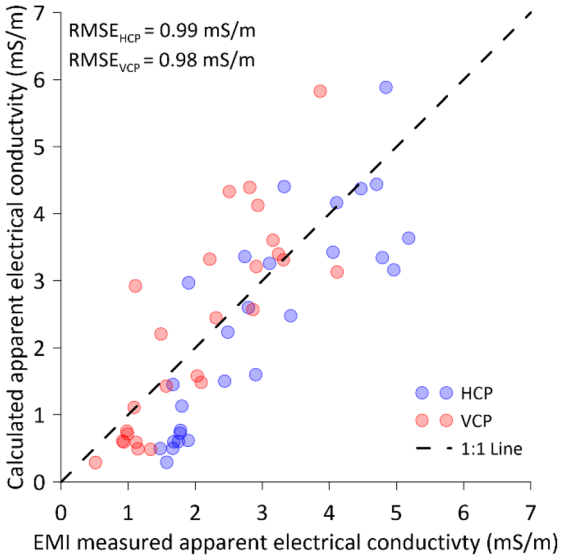

Fig. 6 Scatter plots of electromagnetic induction (EMI) measured *versus* calculated apparent electrical conductivity (ECa) of block 1 data while adjusting the exponents (*m* and *n*) of Archie's petrophysical. The dashed lines correspond to the 1 : 1 line.

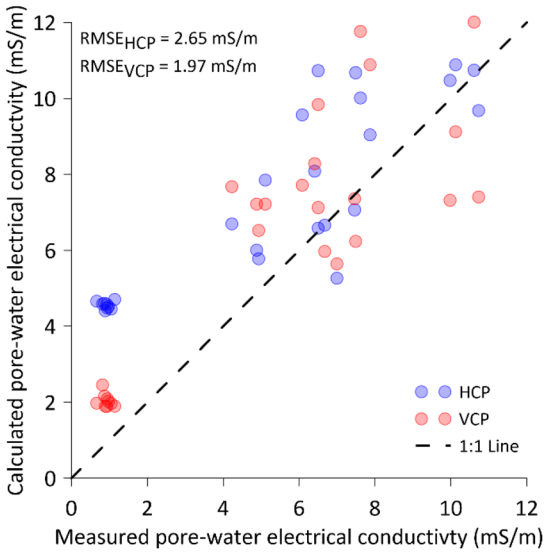

Fig. 7 Scatter plots of measured pore water electrical conductivity (ECw) *versus* Archie's model calculated (using adjusted exponents) ECw of Block 2 data. The dashed lines correspond to the 1 : 1 line.

Archie parameters obtained in our study ($m = 0.67$, $n = 0.11$) are notably lower than typical laboratory-derived values. This discrepancy likely reflects the differences between laboratory and field conditions. In the field, site-specific factors like heterogeneous soil structure, variable pore connectivity, surface conduction, and environmental factors can influence electrical properties differently than in controlled laboratory settings reported in the literature. A lower *m* suggests a relatively well-connected pore network, while the unusually low *n* may indicate that electrical conductivity is less sensitive to water content variations in this context, possibly due to ionic conduction along grain surfaces. These atypical exponent values emphasize the need for caution when generalizing our model beyond the calibration site. While a generalized value for sandy soil texture was considered, no direct laboratory analysis was conducted to determine site-specific exponents based on actual texture (sand, silt and clay percentage). Additionally, the model relied on proxy data from GPR and EMI rather than direct standard laboratory measurements, which may introduce some uncertainty. These factors collectively may contribute to the unusually low parameter values obtained in the field. Therefore, we are also investigating modifications to the model structure and considering complementary measurements to improve the robustness and generalizability of our approach. The consistency of these solver-adjusted exponent values for both VCP and HCP datasets further supports their robustness for the soil tested at the study site.

Applying the adjusted exponents to the Block 2 dataset for estimating ECw from EMI-measured ECa resulted in varying levels of accuracy. The RMSE for the VCP data was 1.97 mS m^{-1}, while the HCP data had a slightly higher RMSE of 2.65 mS m^{-1}. These values indicate a reasonable fit with the measured ECw, particularly given the variability inherent in field conditions compared to more controlled laboratory settings (Fig. 7). In lower ECw ranges (BKG data), the calculated values tended to overestimate measured ECw, an effect more pronounced in the HCP data (Fig. 7). As ECw values increased, data points became more scattered around the 1 : 1 line, continuing the trend of overestimation (Fig. 7). This discrepancy highlights the challenge of accurately predicting conductivity values in field conditions, even with optimized parameters.

4.4. Comparison of the stochastic approach and the deterministic approach

The Bland–Altman plot compares the differences between the measured and predicted ECw values (*y*-axis) against their averages (*x*-axis) for both stochastic and deterministic approaches. This analysis provides insights into how well the predictions align with actual measurements. For the stochastic approach, the mean difference (bias) is nearly zero in both the HCP (−0.7 mS m^{-1}) and VCP (−0.3 mS m^{-1}) configurations, indicating minimal bias with a slight tendency to overestimate ECw compared to measured values (Fig. 8). The limits of agreement (LOA), representing the range where most differences between predicted and measured values fall, extend from approximately −3.7 mS m^{-1} to 2.3 mS m^{-1} for HCP and −2.9 mS m^{-1} to 2.3 mS m^{-1} for VCP. This suggests that most predictions made by the stochastic approach are within these ranges, indicating strong overall performance within the 95% confidence level. The slight average difference and relatively narrow LOA demonstrate the high predictive accuracy of the stochastic approach (Fig. 8).

In contrast, the deterministic approach exhibits a larger bias of −2.0 mS m^{-1} for the VCP configuration, indicating a systematic overestimation of ECw. The HCP configuration

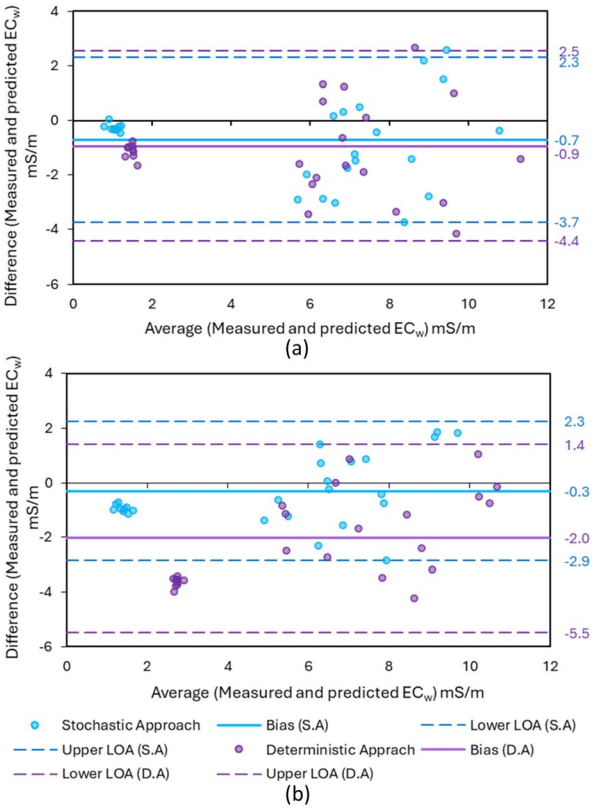

Fig. 8 Bland–Altman plot of pore-water electrical conductivity (ECw) (a) horizontal coplanar (HCP) developed stochastic and deterministic models, and (b) vertical coplanar (VCP) developed stochastic and deterministic models. S.A. – stochastic approach and D.A. – deterministic approach. Solid lines represent the bias, and dash lines represent the limit of agreement 95%.

shows a smaller bias of −0.9 mS m^{-1} (Fig. 8). The LOA for the HCP-based model range from −4.4 mS m^{-1} to 2.5 mS m^{-1}, whereas those for the VCP-based model range from −5.5 mS m^{-1} to 1.4 mS m^{-1}. These wider LOA suggest greater variability in predictions, indicating less consistency compared to the stochastic approach. Overall, the Bland–Altman plots reveal that both approaches generally provide reasonable predictions of ECw, but the stochastic approach achieves better agreement with measured values due to lower bias and a narrower LOA.

The observed negative bias in the Bland–Altman plot (ranging from 0 to −2 dS m^{-1}) suggests that the deterministic method tends to systematically overestimate ECw. This bias can be largely attributed to the inherent differences between the data sources used for model calibration and testing. Specifically, the measured ECw values were obtained through point-based laboratory analysis of soil samples, whereas the calculated values were derived from geophysical proxies (EMI and GPR), which integrate signals over a larger soil volume. Additionally, this mismatch in measurement scale can lead to inconsistencies, particularly when local heterogeneity is present. Moreover, the deterministic model relies on indirect proxy variables rather than direct salinity measurements, making it more susceptible to uncertainties introduced by variations in soil properties, such as moisture content or texture, which can influence sensor response but are not explicitly accounted for in the model. These factors collectively contribute to the systematic bias observed.

Furthermore, the *F*-statistics analysis compares the variance of the developed models under both stochastic and deterministic approaches against the measured ECw (Table 4). The observed *F*-values for all models are compared with the critical *F*-value of 2.19 at a 0.05 significance level (DF = 53). Since all *p*-values exceed 0.05, there is no statistically significant difference in the variances between the developed models (both approaches) and the measured data (Table 4). This consistency reinforces the reliability of both approaches in replicating real-world conditions.

Despite acceptable accuracy in predicting ECw under field conditions, several limitations should be acknowledged for stochastic and deterministic approaches. The performance of the stochastic approach depends on the quality and representativeness of input data in the MLR model. Its effectiveness may decrease under different environmental conditions or when soil properties change. Additionally, this method relies on sensor-derived proxies rather than direct measurements of the state variables. For example, SWC was estimated using the GPR direct ground wave method instead of standard gravimetric sampling, which introduces an average error of 2–5%, depending on site conditions. Although a formal sensitivity or uncertainty analysis was not conducted, this level of error may influence the accuracy of ECw predictions, particularly in conditions where slight variations in SWC significantly affect salinity estimates. Since GPR measurements reflect bulk soil conditions and require empirical calibration, any error in SWC estimation can propagate through the predictive model. While our focus was on assessing the broader applicability of EMI and GPR as non-invasive tools, we recognize that incorporating methods such as Monte Carlo simulations or uncertainty propagation techniques in future studies would help to better quantify and manage prediction error linked to input data variability.

Further refining the exponents used in Archie's equation to better reflect field conditions could improve the precision of

Table 4 The *F*-statistics table summarizes the variance comparison between the developed models[a]

Approach	$F_{observed}$	*p*-value
Stochastic approach		
VCP model	0.96	0.915
HCP model	1.57	0.259
Deterministic approach		
VCP model	1.09	0.815
HCP model	1.96	0.092

[a] DF = 53; α = 0.05; $F_{critical}$ 2.19.

predicted ECa or ECw values, particularly in capturing the variability observed in the field data. Similarly, EMI measurements, while useful for site-specific predictions, may introduce variability due to their sensitivity to site conditions. EMI provides a depth weighted estimate of electrical conductivity over a broad footprint, which may not correspond closely with point-scale ECw measurements. Another challenge with the stochastic approach is the risk of overfitting, where the model performs well on the current dataset but may fail to generalize to other locations or conditions, given the high variability of ECw.

On the other hand, although well-established and extensively validated through laboratory experiments under highly controlled conditions, the deterministic approach faces challenges when applied in the field. Laboratory-estimated model parameters, such as exponents, may not provide the same level of accuracy in the field due to differences in sample volume between laboratory and field conditions, as well as inherent variability present in field settings. This study emphasizes the need for field calibration of laboratory-derived fitting parameters to account for field uncertainties, including soil structure, texture, and the presence of roots and stones. The significant deviation of adjusted fitting parameters from literature values further underscores the challenges of directly applying lab-based models to field conditions.

Looking ahead, the stochastic approach should be tested across diverse field conditions, including varying soil textures, SWC levels, and ECw and ECa conditions. For the deterministic approach, establishing site-specific fitting parameters tailored to specific fields or soils will be crucial before field applications. These fitting parameters can then be refined using mathematical optimization techniques, such as the solver function, to enhance predictive accuracy and reliability in practical applications.

5 Conclusions

This study explored two predictive approaches—stochastic and deterministic—to estimate pore-water electrical conductivity (ECw) based on electromagnetic induction (EMI) and ground-penetrating radar (GPR) measurements, and evaluated their effectiveness. The results revealed that the stochastic approach generally produced predictions that were more closely aligned with actual ECw measurements compared to the deterministic approach. Furthermore, variance analysis confirmed that the variability in predictions from both methods did not significantly differ from that of the measured data, demonstrating consistent model performance.

Utilizing proxies from GPR and EMI to estimate ECw at the field scale presents a novel and practical solution to the challenges of measuring ECw, which is both temporally dynamic and difficult to quantify. The stochastic and deterministic approaches applied in this study show strong potential for field applications, offering promising insights into their utility. However, further refinement is needed to enhance their reliability and robustness. Future research should focus on optimizing model parameters such as Archie's equation exponents, calibration coefficients, and soil-specific inputs through site-specific field and lab validation. Incorporating additional data layers such as soil texture, soil water dynamics, and salinity inputs can further enhance model performance. Developing hybrid integrated approaches that combine both deterministic and stochastic methods may offer the most promising path forward, enabling accurate and consistent ECw estimation under varying environmental and management conditions. These advancements will support more effective use of GPR and EMI techniques in applications such as precision irrigation, salinity management, and digital soil mapping.

This study introduces a new hypothesis for future research: integrating GPR and EMI techniques with stochastic and deterministic modeling approaches could provide a reliable and innovative framework for estimating ECw in large-scale fields.

Author contributions

SP: conceptualization, data curation, formal analysis, investigation, methodology, software, visualization, writing – original draft; SL: conceptualization, supervision, validation, writing – review & editing; MK: validation, writing – review & editing; MC: supervision, validation, writing – review & editing; CS: supervision, validation, writing – review & editing; LG: conceptualization, funding acquisition, investigation, methodology, project administration, resources, supervision, validation, writing – review & editing.

Conflicts of interest

There are no conflicts to declare.

Data availability

The data supporting this article have been included as part of the SI.

The supplementary information includes two tables; the first table contains field- and laboratory-measured data, along with calculated values and second table contain measured and estimated pore-water electrical conductivities derived from both stochastic and deterministic approaches. See DOI: **https://doi.org/10.1039/d5va00121h**.

Appendix

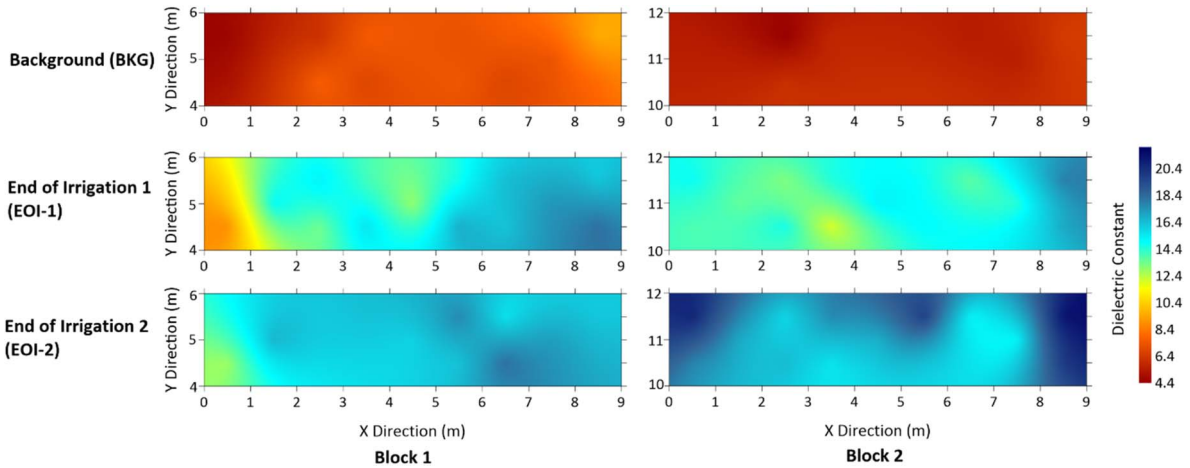

Fig. 9 Ground-penetrating radar estimated dielectric constant map of Blocks 1 and 2 under background (BKG), end of irrigation 1 (EOI-1), and end of irrigation 2 (EOI-2).

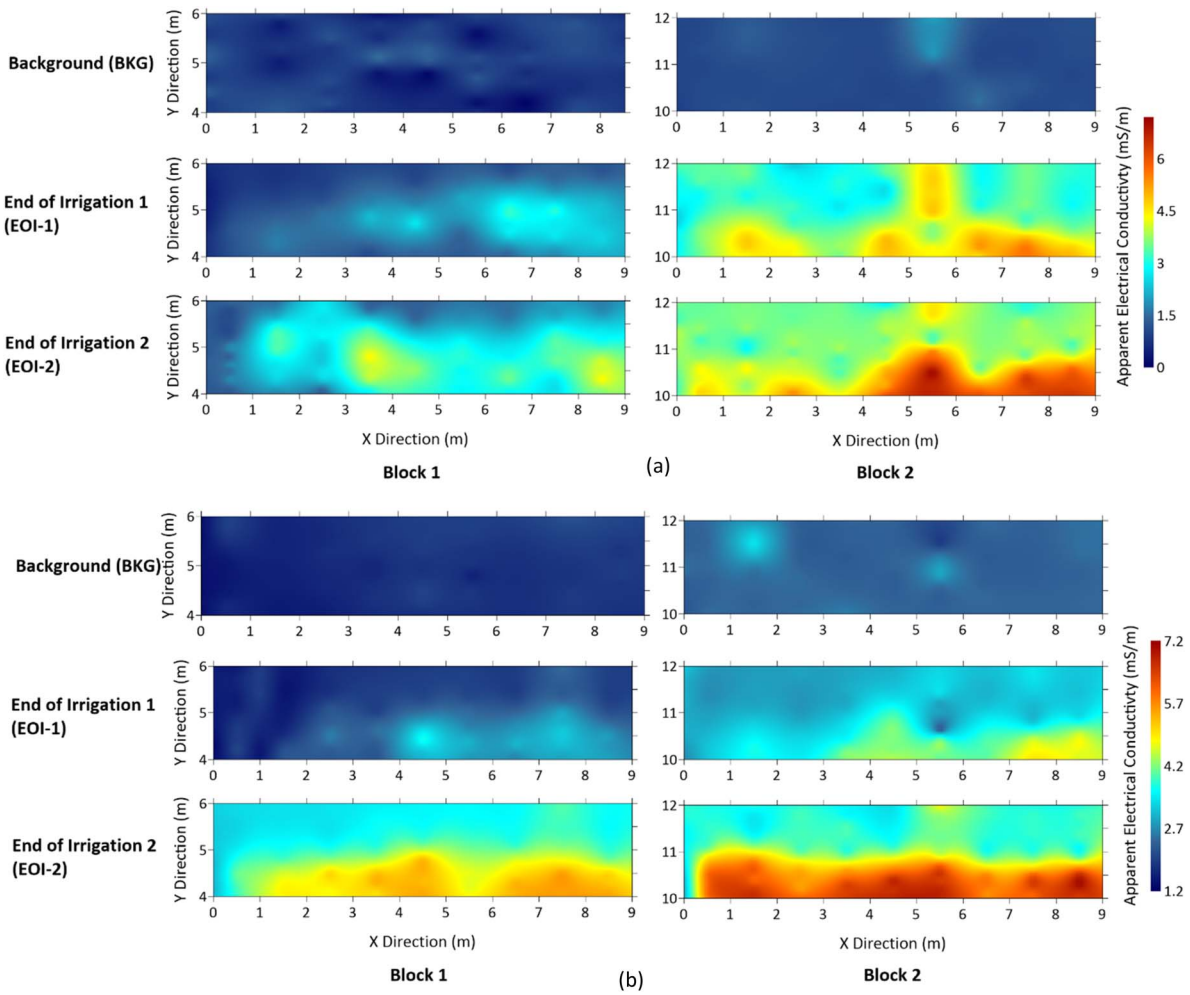

Fig. 10 Electromagnetic Induction measured apparent electrical conductivity map of Blocks 1 and 2 under background (BKG), end of irrigation 1 (EOI-1), and end of irrigation 2 (EOI-2), (a) vertical coplanar and (b) horizontal coplanar.

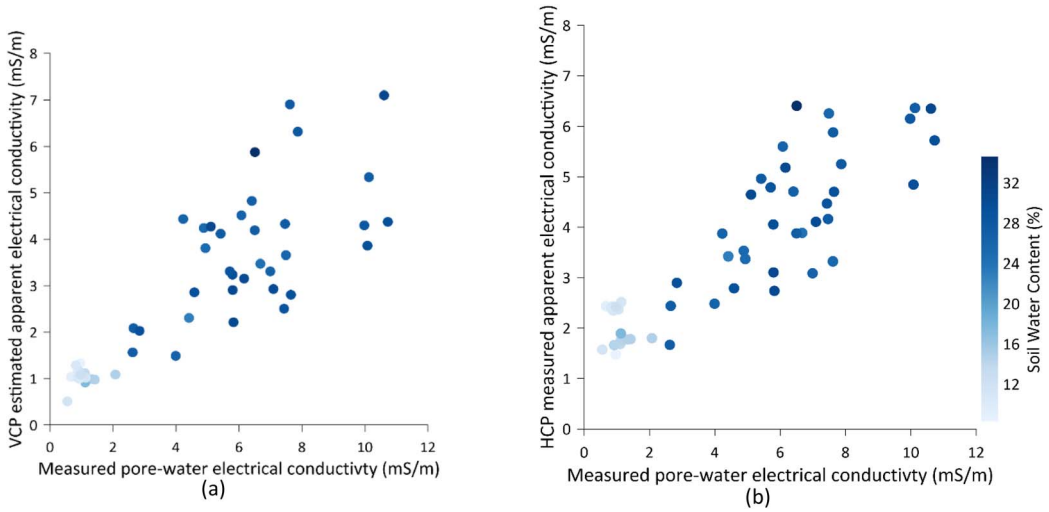

Fig. 11 Apparent electrical conductivity (ECa) measured from electromagnetic induction (EMI); (a) VCP and (b) HCP, as a function of measured pore-water electrical conductivity (ECw) and soil water content (SWC), based on the Rhoades's petrophysical model.

Acknowledgements

Authors would like to acknowledge the financial support provided by the Natural Sciences and Engineering Research Council of Canada, Discovery Grant (NSERC-DG): RGPIN-2019-04614, Industry, Energy and Innovation (IET) of the Government of Newfoundland and Labrador, Grant: 5404-1962-102, and Grenfell Campus, Memorial University of Newfoundland. The authors would like to express sincere gratitude to Adrian Reid and the other staff members of the Department of Fisheries, Forestry, and Agriculture, Government of Newfoundland and Labrador, for their provision and oversight of the research field. The authors extend special appreciation to the Hydrology and Agrogeophysics research group of Grenfell Campus for their assistance in field data collection.

References

1 D. L. Corwin, Soil salinity measurement, in *Encyclopedia of Water Science*, 2003, pp. 852–857.
2 M. G. Eltarabily, A. Amer, M. Farzamian, F. Bouksila, M. Elkiki and T. Selim, Time-lapse electromagnetic conductivity imaging for soil salinity monitoring in salt-affected agricultural regions, *Land*, 2024, **13**, 225.
3 H. Dakak, J. Huang, A. Zouahri, A. Douaik and J. Triantafilis, Mapping soil salinity in 3-dimensions using an EM38 and EM4 soil inversion modelling at the reconnaissance scale in central Morocco, *Soil Use Manage.*, 2017, **33**(4), 553–567.
4 D. L. Corwin and S. M. Lesch, Application of soil electrical conductivity to precision agriculture: Theory, principles, and guidelines, *Agron. J.*, 2003, **95**(3), 455–471.
5 D. L. Corwin and S. M. Lesch, Apparent soil electrical conductivity measurements in agriculture, *Comput. Electron. Agric.*, 2005, **46**(1–3), 11–43.
6 D. L. Corwin and E. Scudiero, Review of soil salinity assessment for agriculture across multiple scales using proximal and/or remote sensors, in *Advances in Agronomy*, ed. D. L. Sparks, Elsevier, Amsterdam, The Netherlands, 2019, vol. 158, pp. 1–130.
7 Y. Fu, R. Horton, T. Ren and J. L. Heitman, A general form of Archie's model for estimating bulk soil electrical conductivity, *J. Hydrol.*, 2021, **597**, 126160, DOI: 10.1016/j.jhydrol.2021.126160.
8 J. Baradaran Motie, M. H. Aghkhani, A. Rohani and A. Lakzian, A soft-computing approach to estimate soil electrical conductivity, *Biosyst. Eng.*, 2021, **205**, 105–120.
9 J. D. Rhoades, D. L. Corwin and S. M. Lesch, Geospatial measurements of soil electrical conductivity to assess soil salinity and diffuse salt loading from irrigation, in *Assessment of Non-point Source Pollution in the Vadose Zone*, Geophysical Monograph, ed. D. L. Corwin, K. Loague and T. .R. Ellsworth, American Geophysical Union, Washington, DC, USA, 1999, vol. 108, pp. 197–215.
10 S. P. Friedman, Soil properties influencing apparent electrical conductivity: a review, *Comput. Electron. Agric.*, 2005, **46**(1), 45–70.
11 B. Aljoumani, J. A. Sanchez-Espigares and G. Wessolek, Estimating pore water electrical conductivity of sandy soil from time domain reflectometry records using a time-varying dynamic linear model, *Sensors*, 2018, **18**(12), 4403, DOI: 10.3390/s18124403.
12 E. Badewa, A. Unc, M. Cheema, V. Kavanagh and L. Galagedara, Soil moisture mapping using multi-frequency and multi-coil electromagnetic induction sensors on managed podzols, *Agronomy*, 2018, **8**(10), 224, DOI: 10.3390/agronomy8100224.
13 L. W. Galagedara, G. W. Parkin and J. D. Redman, An analysis of the ground-penetrating radar direct ground wave method for soil water content measurement, *Hydrol. Process.*, 2003, **17**(18), 3615–3628.
14 L. W. Galagedara, G. W. Parkin, J. D. Redman and A. L. Endres, Assessment of soil moisture content

measured by borehole GPR and TDR under transient irrigation and drainage, *J. Environ. Eng. Geophys.*, 2003, **8**(2), 77–86.

15 J. A. Huisman, S. S. Hubbard, J. D. Redman and A. P Annan, Measuring soil water content with ground penetrating radar: a review, *Vadose Zone J.*, 2003, **2**(4), 476–491.

16 A. Klotzsche, F. Jonard, M. C. Looms, J. van der Kruk and J. A. Huisman, Measuring soil water content with ground penetrating radar: A decade of progress, *Vadose Zone J.*, 2018, **17**(1), 1–9.

17 S. Lambot, J. Rhebergen, I. van den Bosch, E. C. Slob and M. Vanclooster, Measuring the soil water content profile of a sandy soil with an off-ground monostatic ground penetrating radar, *Vadose Zone J.*, 2004, **3**(4), 1063–1071.

18 S. Lambot, L. Weihermüller, J. A. Huisman, H. Vereecken, M. Vanclooster and E. C. Slob, Analysis of air-launched ground-penetrating radar techniques to measure the soil surface water content, *Water Resour. Res.*, 2006, **42**, W11403, DOI: **10.1029/2006WR005097**.

19 C. Mensah, Y. Katanda, M. Krishnapillai, M. Cheema and L. Galagedara, Estimation of soil water content using electromagnetic induction sensors under different land uses, *Environ. Res. Commun.*, 2023, **5**(8), 1–22.

20 J. Minet, P. Bogaert, M. Vanclooster and S. Lambot, Validation of ground penetrating radar full-waveform inversion for field scale soil moisture mapping, *J. Hydrol.*, 2012, **424**, 112–123.

21 S. Pathirana, S. Lambot, M. Krishnapillai, C. Smeaton, M. Cheema and L. Galagedara, Potential of ground-penetrating radar to calibrate electromagnetic induction for shallow soil water content estimation, *J. Hydrol.*, 2024, **633**, 130957, DOI: **10.1016/j.jhydrol.2024.130957**.

22 K. Wu, G. A. Rodriguez, M. Zajc, E. Jacquemin, M. Clément, A. De Coster and S. Lambot, A new drone-borne GPR for soil moisture mapping, *Rem. Sens. Environ.*, 2019, **235**, 111456, DOI: **10.1016/j.rse.2019.111456**.

23 K. Wu, H. Desesquelles, R. Cockenpot, L. Guyard, V. Cuisiniez and S. Lambot, Ground-penetrating radar full-wave inversion for soil moisture mapping in Trench-Hill potato fields for precise irrigation, *Remote Sens.*, 2022, **14**(23), 6046, DOI: **10.3390/rs14236046**.

24 J. Doolittle, M. Petersen and T. Wheeler, Comparison of two electromagnetic induction tools in salinity appraisals, *J. Soil Water Conserv.*, 2001, **56**(3), 257–262.

25 J. Robinet, C. von Hebel, G. Govers, J. van der Kruk, J. P. G. Minella, A. Schlesner, Y. Ameijeiras-Mariño and J. Vanderborght, Spatial variability of soil water content and soil electrical conductivity across scales derived from electromagnetic induction and time domain reflectometry, *Geoderma*, 2018, **314**, 160–174.

26 V. Urdanoz and R. Aragüés, Comparison of Geonics EM38 and Dualem 1S electromagnetic induction sensors for the measurement of salinity and other soil properties, *Soil Use Manag.*, 2012, **28**(1), 108–112.

27 D. De Benedetto, E. Barca, M. Castellini, S. Popolizio, G. Lacolla and A. M. Stellacci, Prediction of soil organic carbon at field scale by regression kriging and multivariate adaptive regression splines using geophysical covariates, *Land*, 2022, **11**(3), 381, DOI: **10.3390/land11030381**.

28 X. Shen, T. Foster, H. Baldi, I. Dobreva, B. Burson, D. Hays, R. Tabien and R. Jessup, Quantification of soil organic carbon in biochar-amended soil using ground penetrating radar (GPR), *Remote Sens.*, 2019, **11**(23), 2874, DOI: **10.3390/rs11232874**.

29 T. Rentschler, U. Werban, M. Ahner, T. Behrens, P. Gries, T. Scholten and K. Schmidt, 3D mapping of soil organic carbon content and soil moisture with multiple geophysical sensors and machine learning, *Vadose Zone J.*, 2020, **19**(1), e20062, DOI: **10.1002/vzj2.20062**.

30 A. Akinsunmade, S. Tomecka-Suchoń, P. Kiełbasa, T. Juliszewski, P. Pysz, J. Karczewski, M. Zagórda and M. GPR, geophysical method as a remediation tool to determine zones of high penetration resistance of soil, *J. Phys.: Conf. Ser.*, 2021, **1782**(1), 012001, DOI: **10.1088/1742-6596/1782/1/012001**.

31 F. Jonard, M. Mahmoudzadeh, C. Roisin, L. Weihermüller, F. André, J. Minet, H. Vereecken and S. Lambot, Characterization of tillage effects on the spatial variation of soil properties using ground-penetrating radar and electromagnetic induction, *Geoderma*, 2013, 207–208.

32 S. Pathirana, S. Lambot, M. Krishnapillai, M. Cheema, C. Smeaton and L. Galagedara, Integrated ground-penetrating radar and electromagnetic induction offer a non-destructive approach to predict soil bulk density in boreal podzolic soil, *Geoderma*, 2024, **450**, 117028, DOI: **10.1016/j.geoderma.2024.117028**.

33 A. Romero-Ruiz, D. O'Leary, E. Daly, P. Tuohy, A. Milne, K. Coleman and A. P. Whitmore, An agro-geophysical modelling framework for the detection of soil compaction spatial variability due to grazing using field-scale electromagnetic induction data, *Soil Use Manage.*, 2024, **40**(2), e13039.

34 P. Wang, Z. Hu, Y. Zhao and X. Li, Experimental study of soil compaction effects on GPR signals, *J. Appl. Geophys.*, 2016, **126**, 128–137.

35 S. Pathirana, S. Lambot, M. Krishnapillai, M. Cheema, C. Smeaton and L. Galagedara, Ground-penetrating radar and electromagnetic induction: Challenges and opportunities in agriculture, *Remote Sens.*, 2023, **15**, 2932, DOI: **10.3390/rs15112932**.

36 C. Ferrara, P. M. Barone, E. Mattei, A. Galli, D. Comite, S. E. Lauro, G. Vannaroni and E. Pettinelli, An evaluation of the early-time GPR amplitude technique for electrical conductivity monitoring, in *Proceedings of the IWAGPR 2013—7th International Workshop on Advanced Ground Penetrating Radar*, 2–5 July 2013, IEEE, Nantes, France, Manhattan, NY, USA, 2013, pp. 1–4.

37 B. Wu, X. Li, K. Zhao, T. Jiang, X. Zheng, X. Li, L. Gu and X. Wang, A Nondestructive Conductivity Estimating Method for Saline-Alkali Land Based on Ground Penetrating Radar, *IEEE Trans. Geosci. Rem. Sens.*, 2020, **58**(4), 2605–2614, DOI: **10.1109/TGRS.2019.2952719**.

38 J. Doolittle, M. Petersen and T. Wheeler, Comparison of two electromagnetic induction tools in salinity appraisals, *J. Soil Water Conserv.*, 2001, **56**, 257–262.
39 G. K. Ganjegunte, Z. Sheng and J. A. Clark, Soil salinity and sodicity appraisal by electromagnetic induction in soils irrigated to grow cotton, *Land Degrad. Dev.*, 2014, **25**(3), 228–235, DOI: **10.1002/ldr.1162**.
40 L. De Carlo, G. A. Vivaldi and M. C. Caputo, Electromagnetic Induction Measurements for Investigating Soil Salinization Caused by Saline Reclaimed Water, *Atmosphere*, 2022, **13**(1), 73, DOI: **10.3390/atmos13010073**.
41 T. Bughici, T. H. Skaggs, D. L. Corwin and E. Scudiero, Ensemble HYDRUS-2D modeling to improve apparent electrical conductivity sensing of soil salinity under drip irrigation, *Agric. Water Manag.*, 2022, **272**, 107813, DOI: **10.1016/j.agwat.2022.107813**.
42 M. G. Eltarabily, A. Amer, M. Farzamian, F. Bouksila, M. Elkiki and T. Selim, Time-Lapse Electromagnetic Conductivity Imaging for Soil Salinity Monitoring in Salt-Affected Agricultural Regions, *Land*, 2024, **13**(2), 225, DOI: **10.3390/land13020225**.
43 S. Gu, S. Jiang, X. Li, N. Zheng and X. Xia, Soil salinity simulation based on electromagnetic induction and deep learning, *Soil Tillage Res.*, 2023, **230**, 105706, DOI: **10.1016/j.still.2023.105706**.
44 D. Moghadas, F. André, E. C. Slob, H. Vereecken and S. Lambot, Joint full-waveform analysis of off-ground zero-offset ground penetrating radar and electromagnetic induction synthetic data for estimating soil electrical properties, *Geophys. J. Int.*, 2010, **182**(3), 1267–1278.
45 G. E. Archie, The electrical resistivity log as an aid in determining some reservoir characteristics, *Trans. AIME*, 1942, **146**, 54–62.
46 J. D. Rhoades, N. A. Manteghi, P. J. Shouse and W. J. Alves, Soil electrical conductivity and soil salinity: new formulations and calibrations, *Soil Sci. Soc. Am. J.*, 1989, **53**, 433–439.
47 J. D. Rhoades, P. A. C. Ratts and R. J. Prather, Effects of liquid-phase electrical conductivity, water content, and surface conductivity on bulk soil electrical conductivity, *Soil Sci. Soc. Am. J.*, 1976, **40**, 651–655.
48 S. C. Gupta and R. J. Hanks, Influence of water content on electrical conductivity of the Soil, *Soil Sci. Soc. Am. J.*, 1972, **36**, 855–857.
49 M. A. Mojid, D. A. Rose and G. C. L. Wyseure, A model incorporating the diffuse double layer to predict the electrical conductivity of bulk soil, *Eur. J. Soil Sci.*, 2007, **58**, 560–572.
50 P. H. Shah and D. N. Singh, Generalized archie's law for estimation of soil electrical conductivity, *J. ASTM Int.*, 2005, **2**, 145–164.
51 R. P. Ewing and A. G. Hunt, Dependence of the electrical conductivity on saturation in real porous media, *Vadose Zone J.*, 2006, **5**, 731–741.
52 P. W. J. Glover, A generalized Archie's law for n phases, *Geophysics*, 2010, **75**, 247–265.
53 P. W. J. Glover, Archie's law—A reappraisal, *Solid Earth*, 2016, **7**, 1157–1169.
54 S. Pathirana, S. Lambot, M. Krishnapillai, C. Smeaton, M. Cheema and L. Galagedara, Integrated ground-penetrating radar and electromagnetic induction techniques for characterizing boreal podzolic soil in western Newfoundland, *Can. J. Soil Sci.*, 2024, **104**(4), 509–513.
55 K. R. Sheets and J. M. H. Hendrickx, Non-invasive soil water content measurement using electromagnetic induction, *Water Resour. Res.*, 1995, **31**, 2401–2409.
56 G. C. Topp, J. L. Davis and A. P. Annan, Electromagnetic determination of soil water content: measurements in coaxial transmission lines, *Water Resour. Res.*, 1980, **16**(3), 574–582.